# Combination of high-performance refractometry and infrared spectroscopy as a probe for chemically induced gelation and vitrification of epoxies



2010 New J. Phys. 12 083036

(http://iopscience.iop.org/1367-2630/12/8/083036)

New Journal of Physics
The open-access journal for physics

# Combination of high-performance refractometry and infrared spectroscopy as a probe for chemically induced gelation and vitrification of epoxies

**U Müller[1,4], M Philipp[1], P-C Gervais[1], W Possart[2], C Wehlack[2], J Kieffer[3], R Sanctuary[1] and J K Krüger[1]**

[1] Laboratoire de Physique des Matériaux, Université du Luxembourg, 162A avenue de la faïencerie, L-1511 Luxembourg, Luxembourg
[2] Fachbereich Werkstoffwissenschaften, Universität des Saarlandes, D-66123 Saarbrücken, Germany
[3] Department of Materials Science and Engineering, University of Michigan, Ann Arbor, MI, USA
E-mail: ulrich.mueller@uni.lu

*New Journal of Physics* **12** (2010) 083036 (17pp)
Received 13 January 2010
Published 17 August 2010
Online at http://www.njp.org/
doi:10.1088/1367-2630/12/8/083036

**Abstract.** A combination of infrared spectroscopy and high-performance refractometry was used to investigate the chemically induced sol–gel and glass transition during the polymerization of epoxies. Representations of the refractive index versus chemical conversion reveal an interesting insight into the optical properties accompanying gelation and vitrification. Whereas the electronic polarizability of the liquid state of small average molecular mass and the glassy state is dominated by the mass density, an unexpected excess polarizability observed during the gelation is attributed to cooperative dipole–dipole interactions.

[4] Author to whom any correspondence should be addressed.

## Contents



## 1. Introduction

The sol–gel transition as well as the structural glass transition belong to the class of isostructural phase transformations [1]. Both phenomena are transitions from one isotropic state to another isotropic state and may appear consecutively in the same material [1]. These transitions are not accompanied by macroscopic symmetry breaking changes. Their coupling to many susceptibilities is weak and they are often superimposed by kinetic effects, which make these transitions hard to detect. An exceptional role is played by the static shear stiffness: both transitions are accompanied by a sudden increase in this quantity. As the static shear stiffness is not easily measured, most research on these transitions is done by means of dynamic mechanical measurements [2]–[7]. Because of the sudden onset of static shear stiffness, i.e. a diverging zero-shear viscosity, gels are sometimes called soft glasses [8]. The physical nature of both types of transitions is still a matter of debate [1], [8]–[11]. This holds true especially if these transitions are driven not by temperature but by a chemical process, like the formation of a polymer network [1], [12]–[16]. In the case of temperature as the driving parameter, both transitions are thermoreversible. However, if the driving parameter is chemical cross-linking at a given temperature, the sol–gel transition is irreversible, while the glass transition can be overcome by increasing temperature.

Most research concerning chemically induced transitions relies either on qualitative static measurements [17] or on dynamic investigations, like rheology, dynamic mechanical analysis or dielectric measurements [7, 15], [18]–[22]. In the field of chemically induced glass transitions, calorimetry plays a major role, too [1], [23]–[27]. However, further experimental probes could also contribute to the comprehension of chemically induced structural formation. For this purpose, in the current article, two optical methods with complementary information content are combined. While infrared spectroscopy yields information about the chemical aspects of the polymerization, such as the chemical conversion [24], [28]–[30], refractometry is able to deliver insight into the structural aspects as expressed by dielectric properties [31]–[43]. Our main interest in the refractive index results from its highly precise, quasi-static physical nature, which is essentially measured in linear response. Due to the high probe frequencies, relaxational dynamics linked to the sol–gel and glass transitions are not relevant. Moreover, the refractive index is highly sensitive to network formation as this process affects different contributions of electronic polarizability at optical frequencies. Among those are counted the electric dipole number density, which is roughly proportional to the mass density, the strengths of the electronic dipoles, the molecular shape and the molecular arrangement [36]–[38], [44].

As model systems, we chose different epoxy compositions based on the resin diglycidyl ether of bisphenol A (DGEBA) and the hardener diethylene triamine (DETA), which undergo either no, one or both isostructural phase transitions during isothermal polymerization.

In the following, we focus on the evolution of the refractive index during the chemically driven gelation and vitrification of the different epoxy compositions. Special interest is paid to the role of mass density and the other aforementioned polarizability contributions during the initial liquid state of small molecular weight, the gelation and the glassy state.

## 2. Experimental

### *2.1. Samples and sample preparation*

The epoxy system consists of the resin DGEBA DER 332 from Dow Chemical and (at room temperature) the liquid hardener diethylene triamine (DETA) from Fluka Chemie GmbH (Switzerland). The functional chemical groups of the resin are two oxirane rings. The functional groups of the hardener are five amine hydrogens, distributed on two primary and one secondary amine groups.

A wide range of mass ratios of the constituents are chosen to cover all possible phase transition scenarios: no transition, only a sol–gel transition and a sol–gel transition followed by a glass transition. The chosen mass ratios DGEBA/DETA are (100/3, 5, 7, 10, 12, 14, 18, 30, 40, 61, 80) with (100/12) reflecting the stoichiometric ratio.

First the constituents are degassed. Then sample preparation is performed by mixing the constituents for 5 min by means of a magnetic stirrer at 55 °C in order to exceed the melting temperature of DGEBA. After mixing, the samples are cooled down quickly to ambient temperature in a water bath and applied to the infrared spectrometer and the refractometer. In this way, simultaneous measurements can always be performed on the same sample batch. The isothermal polymerizations are studied at 295 K. The moment of adding the hardener to the resin is taken as the start time of polymerization (all times in the graphical representations of the measured data are shifted appropriately). The problem of removing glassy adhesives from the prisms after room temperature polymerization is solved by applying a suitable treatment with the solvent dimethyl formamide.

### *2.2. Experimental methods*

Both experimental techniques, the Abbe refractometry and the attenuated total reflection infrared spectroscopy, are based on the total reflection of an electromagnetic wave incident from the prism to the optically less dense sample. Fresnel's formulae accurately describe the relevant reflection and absorbance processes [45]. The evanescent wave that propagates in the case of total reflection along the interface before entering the prism again carries the information about the sample's optical properties. The evanescent wave's penetration depth into the sample $d_{\mathrm{depth}}$ depends on the vacuum wavelength $\lambda_0$ and the angle of incidence $\varphi$ of the incident electromagnetic wave and on the ratio between the refractive indices $n_{\lambda_{0\,\mathrm{S/P}}} = n_{\lambda_{0\,\mathrm{Sample}}}/n_{\lambda_{0\,\mathrm{Prism}}}$,

$$d_{\mathrm{depth}} = \frac{\lambda_0}{2\pi \cdot n_{\lambda_{0\,\mathrm{Prism}}}\sqrt{\sin^2(\varphi) - n^2_{\lambda_{0\,\mathrm{S/P}}}}}. \tag{1}$$

Consequently, information about the sample's optical properties is obtained from the sample layer adjacent to the prism. This layer's thickness lies in the several hundred nanometer range for refractometry and several micrometer range for infrared spectroscopy. For the infrared spectroscopic investigations, the imaginary part of the refractive index is an especially important property as it allows the description of the wavelength-dependent absorbance of the incident electromagnetic wave via excitation of molecular degrees of vibration.

*2.2.1. Refractometry.* The used high-precision refractometer Abbemat from Anton Paar OptoTec GmbH (Germany) possesses the high absolute accuracy of $10^{-5}$ and a relative accuracy of $10^{-6}$. The refractometer's optical wavelength equals 589.3 nm (sodium D-line). The measurement chamber was specially sealed in order to avoid additional demixing processes of the reactants because of moisture [46]. The temperature stabilization of the measurement chamber is better than 0.1 K.

The refractive index is related to the dielectric susceptibility at optical frequencies $\varepsilon^{\infty}$ via $n = \sqrt{\varepsilon^{\infty}}$. Note that generally no simple relationship exists between the refractive index and the molecular structure in terms of mass density, being roughly proportional to the electronic dipole number density, and other contributions of electronic polarizability at optical frequencies. Relevant contributions of the latter type may be the strength of the dipoles at optical frequencies, the molecular shape and the molecular arrangement [36]–[38], [44].

Although there is no model relating mass density $\rho$ and refractive index $n$ for polymers, for many systems a good approximation is given by the well-known Lorenz–Lorentz [33, 34] relation,

$$\rho = \frac{1}{r} \cdot \frac{n^2 - 1}{n^2 + 2}, \tag{2}$$

where $r$ is the specific refraction. The specific refraction roughly reflects molecular properties like molecular shape, arrangement and dipole strength. In the surely approximate frame of the group contribution method, the specific refraction, considered from the contributions of chemical groups, is almost a constant during the polymerization of epoxies at ambient temperature [1, 47].

*2.2.2. Infrared spectroscopy.* All measurements were carried out by the technique of attenuated total reflection on a Biorad/Digilab FTS 3000 Excalibur infrared spectrometer. The modification of the spectrometer consisted in the automation of the detector's cooling. Software-controlled recording of the infrared spectra took place every 15 min during the polymerization of the samples. The parameters of the measurement configuration were s-polarization of the incident beam, angle of incidence $\varphi = 60^{\circ}$, and a prism made of zinc selenide [28, 29].

The calculation of the chemical conversion from the infrared spectra is described in detail in [28, 29]. The temporal diminishing of a band's height, belonging to a molecular group that reacts during the polymerization, is determined. As usual, the oxirane band at 915 $\mathrm{cm}^{-1}$ is chosen for this purpose. For each spectrum, the height of the oxirane band $h_{\mathrm{oxirane}}(t)$ is divided by the height of a reference band, the phenylene band at 1510 $\mathrm{cm}^{-1}$ $h_{\mathrm{phenylene}}(t)$, which is independent of the polymerization process. Firstly, this manipulation allows for excluding atmospheric influences on the evaluation resulting, for example, from small temperature fluctuations inside the measurement chamber. Secondly, as the refractive index grows during

the polymerization, the penetration depth of the beam into the sample increases continuously, i.e. also the information volume. This effect is accounted for by the division of the oxirane band's height by that of the reference band $h_{\mathrm{phenylene}}(t)$.

Finally, the chemical conversion, given in per cent, equals

$$u(t) = \left[1 - \frac{h_{\mathrm{oxirane}}(t)/h_{\mathrm{phenylene}}(t)}{h_{\mathrm{oxirane}}(t = 0\,\mathrm{h})/h_{\mathrm{phenylene}}(t = 0\,\mathrm{h})}\right] \times 100. \tag{3}$$

The heights $h_{\mathrm{oxirane}}(t = 0\,\mathrm{h})$ and $h_{\mathrm{phenylene}}$ $(t = 0\,\mathrm{h})$ are estimated by a superposition of the spectra of the reactants [28, 29].

The evaluation of the chemical conversion $u$ suffers an absolute error lower than 8%, and the relative error is significantly lower [28, 29]. In addition, the temperature of the measurement chamber may be subject to long-term variations of several tenths of a kelvin around 295 K. According to experience with temperature-modulated calorimetry, the influence of these fluctuations can be regarded as non-significant for the general polymerization process. For understoichiometric compositions, i.e. below (100/12), the chemical conversion is calculated with respect to the maximum possible oxirane consumption.

## 3. Results and discussion

For the sake of clarity, only the datasets of a representative selection of compositions are displayed in some figures; but all of them are taken into account for the general discussion. Figure 1(a) shows the temporal evolution of the chemical conversion for a wide-stretched range of compositions of the reactants DGEBA and DETA measured at room temperature $T = 295\,\mathrm{K}$. All curves roughly show the same time dependence: at the beginning of the polymerization process they increase more or less steeply and tend to become asymptotic for longer polymerization times.

Room-temperature-polymerized epoxy mixtures based on DGEBA and DETA are known to vitrify in the neighborhood of the stoichiometric composition. As vitrification strongly hinders the chemical reaction, it can be assumed that all systems that do not reach a chemical conversion of 100% vitrify. In figure 1(a), this statement is valid for the compositions (100/7), (100/14) and (100/30). Under strongly understoichiometric and overstoichiometric conditions, a chemically induced glass transition is no longer possible at ambient temperature and thus the degree of polymerization is expected to develop to $u = 100\%$ [7, 15, 16]. The latter behavior is observed for the epoxies (100/5), (100/40) and (100/61). Hence the habit and especially the asymptotic end values of the curves presented in figure 1(a) give indeed a first hint of which systems undergo a chemically induced glass transition during polymerization at 295 K. In contrast, no hints regarding chemically induced sol–gel transitions are obtained from the temporal development of the chemical conversion.

A deeper insight into the transition behavior accompanying the polymerization process is gained from calculations of the chemical reaction velocity versus the conversion $v_r(u) = (\mathrm{d}u/\mathrm{d}t)\,(u)$ that represents the kinetics of the polymerization process. All chemical reaction velocity curves $v_{\mathrm{r}}(u)$ indicated in figure 1(b) follow the same general shape: they start at a finite value, go through a maximum and tend towards zero afterwards. The increase in $v_{\mathrm{r}}(u)$ for low conversions is attributed to catalysis of the epoxy reaction provoked by the rising number of

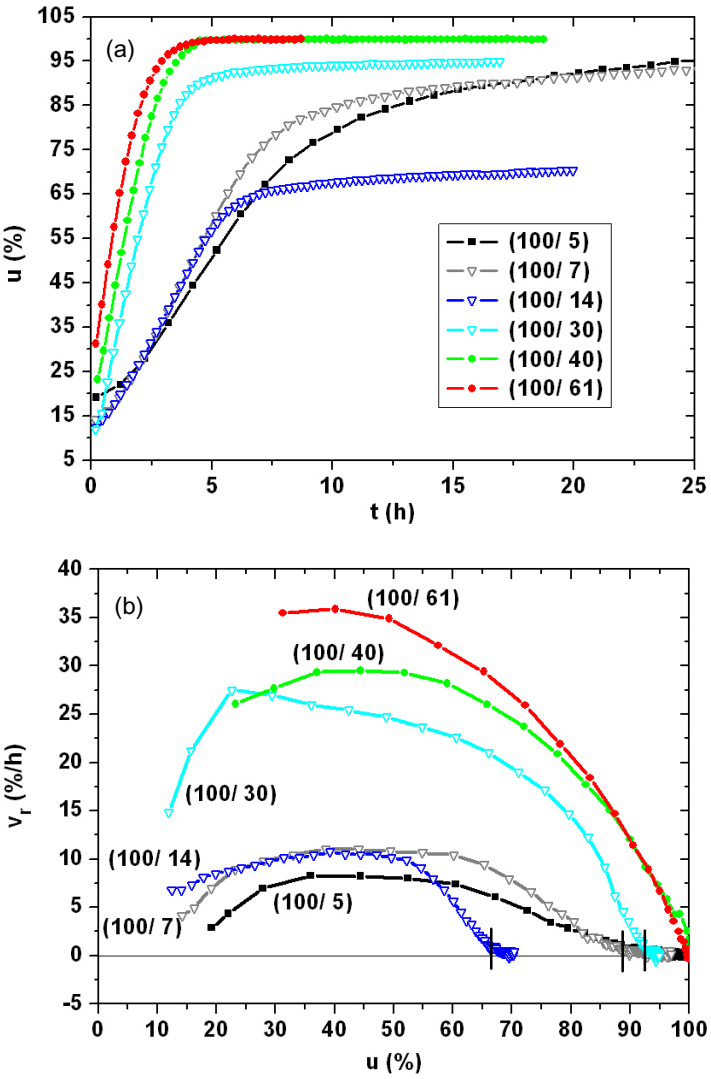


**Figure 1.** (a) Temporal behavior of the chemical conversion and (b) chemical reaction velocity $v_r$ versus chemical conversion $u$ for a representative selection of epoxy compositions at 295 K. The black vertical bars indicate the strong change in slope of $v_r(u)$ for the compositions (100/7), (100/14) and (100/30).

hydroxyl groups [16, 24, 30, 48, 49]. Vitrifying compositions exhibit an inflection point and a subsequent strong change in slope on approaching $v_r(u) = 0\%\,h^{-1}$. This strong change in slope, marked by the black bars in figure 1(b), is interpreted as the onset of the chemically induced glass transition. The finite value of the $v_r(u)$ curves after the glass transition shows that the polymerization process still proceeds in the glassy network. In other words, molecular transport and network formation are not completely stopped by vitrification. The strongly overstoichiometric systems (100/40) and (100/61), which according to their visco-elastic consistency surely do not vitrify during room temperature curing, go straight to $v_r(u) = 0\%\,h^{-1}$. Figure 1(b) suggests that the system (100/30) still freezes and that the epoxy (100/5) is at least close to freezing.

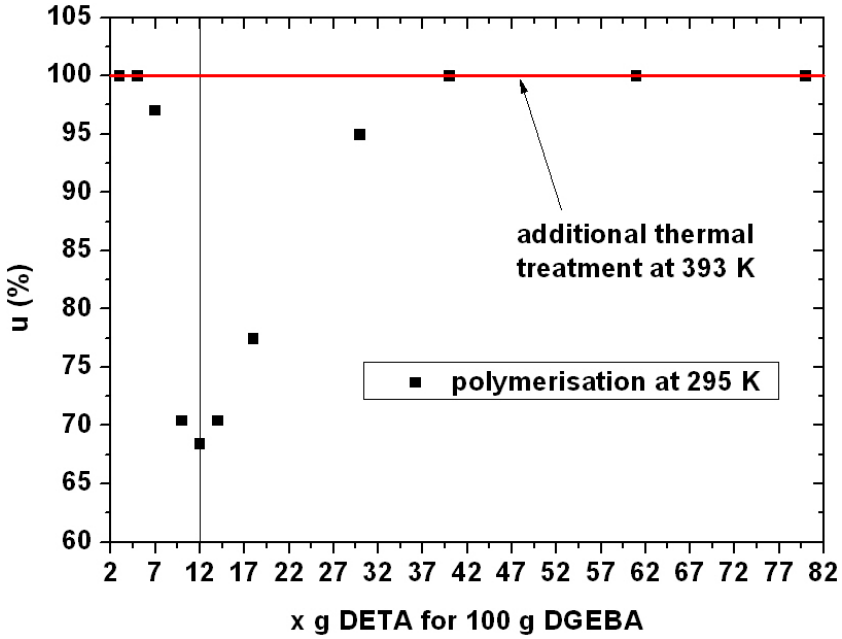


**Figure 2.** Black squares: chemical conversion $u$ versus DETA concentration $x$ for all investigated epoxy mixtures after room temperature polymerization. The red line indicates the chemical conversion of 100% determined after post-polymerization for all samples.

As deduced from the asymptotic $u(t)$ values of figure 1(a), the maximum degree of polymerization at 295 K is strongly reduced in the range of the stoichiometric composition (100/12). The asymptotic values of all room-temperature-polymerized compositions are plotted in figure 2 as black squares. The red line of the same figure corresponds to the chemical conversion of 100% measured after post-polymerization at 393 K for 1 h, a treatment that is known to achieve the complete possible consumption of the oxirane groups. The significant deviation between the datasets of the room-temperature-polymerized and the post-polymerized samples suggests that the aforementioned glass transition occurs probably in the concentration range of (100/7) to (100/30).

Simultaneously to the infrared measurements, the evolution of the refractive index $n(t)$ was recorded for all compositions. Unfortunately, the continuous and monotonous habits of the $n(t)$ curves shown in figure 3 are rather unspectacular concerning evidence for chemically induced sol–gel or glass transitions. Figure 3 shows that there is a systematic increase in the initial slope of $n(t)$ and a systematic decrease in the starting value $n(t = 0)$ with increasing DETA concentration. The former reflects the increase in reaction velocity already depicted in figure 1(b).

As the chemical conversion rather than the polymerization time reflects the state of the chemical network formation, we plot in figure 4 the refractive index versus chemical conversion $n(u)$. Figure 4(a) contains the curves for all studied epoxies that vitrify, and figure 4(b) those of the other systems. These refractive index curves $n(u)$ show features that are not visible in the temporal representations of either $n(t)$ or $u(t)$.

The curves in figure 4 can be divided into up to three distinctive conversion intervals as exemplarily shown for the epoxy (100/30) in figure 4(a). In a first conversion interval (I1),

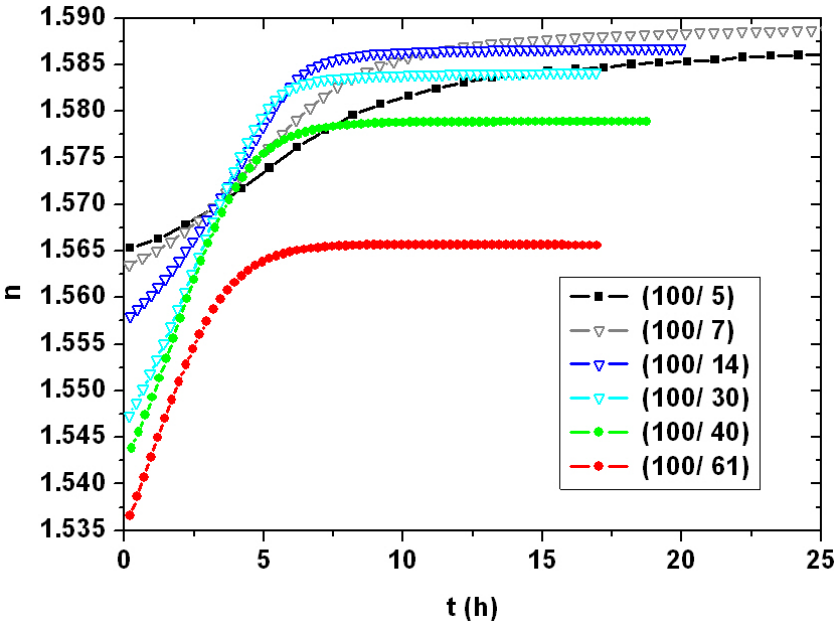


**Figure 3.** Temporal evolution of the refractive index for a representative selection of epoxy compositions at 295 K.

which is a common feature of all compositions, the evolution of the refractive index behaves almost linearly. Mathematically, this linear regime I1 can be described by $n|_x^{\mathrm{I1}}(u) = a_x + b_x \cdot u$, where $a_x$ and $b_x$ are specific constants for the composition $(100/x)$. The extrapolated intercept values $a_x$ agree well with predictions based on a linear volume mixing rule concerning the refractive indices of both epoxy reactants (see table 1). The predicted values are slightly lower than the extrapolated values. At this point it cannot be decided whether the model is unsuitable or whether the volume additivity is violated.

Except for the strongly understoichiometric compositions (100/3) and (100/5), there is a subsequent polymerization range (I2), where the $n(u)$ curves increase in a nonlinear way with $\mathrm{d}n|_x^{\mathrm{I2}}/\mathrm{d}u > b_x$. For the vitrifying compositions, a third range (I3) is observed in which the $n|_x(u)$ curves flatten after the preceding nonlinear increase. This flattening results in a slope of $n|_x^{\mathrm{I3}}(u)$ being smaller than $b_x$.

The different behavior in slope observed for the three intervals suggests that the increase in the refractive index with the chemical conversion $u$ is determined by several optical polarization mechanisms being specific to I1, I2 and I3. As stated in section 2, qualitatively there are a number of contributions to the refractive index: the molecular dipole strength, the molecular shape and arrangement, and the dipole number density being roughly proportional to mass density. The goal of the following discussion is to tentatively relate the measured evolution of the refractive index to different structural formation processes, including the phase transitions accompanying the polymerization.

The interpretation of interval I3 seems the clearest and most obvious compared with the others. As the onset of flattening at the beginning of interval I3 apparently coincides with the kink in the reaction velocity $v_{\mathrm{r}}(u)$ (compare the black vertical bars in figures 1(b) and figure 4(a)), this flattening is attributed to the chemically induced glass transition. Since a rather rigid molecular network has formed during the ongoing isothermal polymerization in

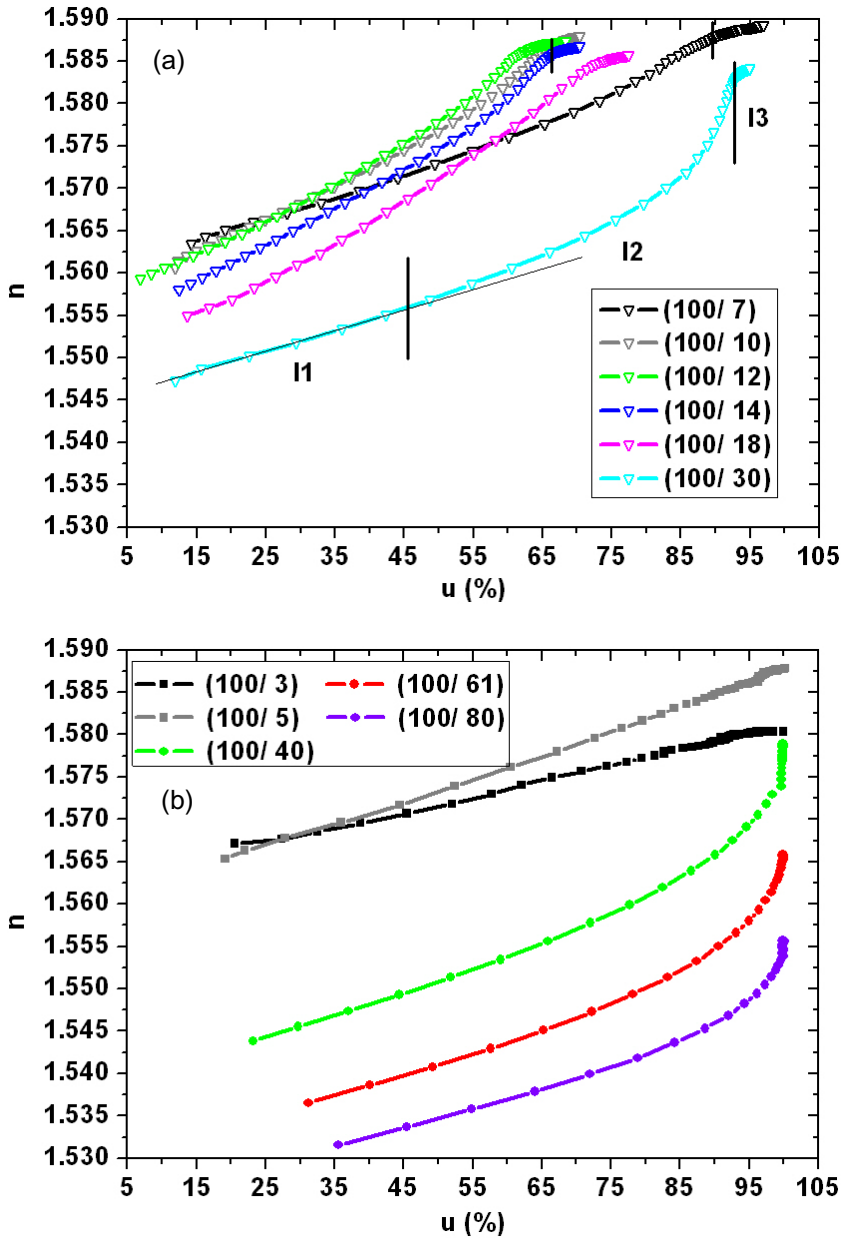


**Figure 4.** Refractive index $n$ versus chemical conversion $u(a)$ for the glass-forming epoxies and (b) for the non-glass-forming epoxies. For the system (100/30), the intervals I1–I3 are exemplarily indicated.

the glassy state, the volume shrinkage is much more hindered in that state than in the liquid or gel state. Thus, in the course of the chemically induced vitrification and in the glassy state, $n(u)$ is dominated by the saturation of the mass density. The current investigations do not allow an interpretation of the remaining finite slope $\mathrm{d}n|_x^{\mathrm{I3}}/\mathrm{d}u$ in the glassy state. It may be dominated either by a slight increase in mass density or by changes in molecular polarizability at an almost constant mass density.

In order to get a clearer view of the influence of the mass density $\rho(u)$ on $n(u)$, for an epoxy-based nanocomposite, the role of nanoparticles in the refractive index evolution $n(u)$ is

**Table 1.** Investigated compositions: mass ratios of resin DGEBA to hardener DETA, molar ratios of the functional groups oxirane and amine, extrapolated $n(u = 0)$-values, estimated $n(u = 0)$-values according to a linear volume mixing rule of the refractive indices of DETA ($n = 1.4846$) and DGEBA ($n = 1.5688$), and Flory–Stockmayer prediction [12, 16] of the critical chemical conversion for the sol–gel transition $u_{sg}$.

| Mass ratio DGEBA/DETA | Molar ratio oxirane amine/hydrogens | $n(u = 0)$ extrapolated | $n(u = 0)$ calculated | $u_{sg}$ Flory–Stockmayer |
|---|---|---|---|---|
| 100 : 3 | 1 : 0.25 | 1.5631 | 1.5658 | 100% |
| 100 : 5 | 1 : 0.42 | 1.5607 | 1.5640 | 77% |
| 100 : 7 | 1 : 0.58 | 1.5601 | 1.5622 | 65% |
| 100 : 10 | 1 : 0.83 | 1.5570 | 1.5596 | 54% |
| 100 : 12 | 1 : 1 | 1.5568 | 1.5580 | 50% |
| 100 : 14 | 1 : 1.17 | 1.5528 | 1.5565 | 54% |
| 100 : 18 | 1 : 1.5 | 1.5493 | 1.5536 | 61% |
| 100 : 30 | 1 : 2.5 | 1.5449 | 1.5462 | 79% |
| 100 : 40 | 1 : 3.33 | 1.5370 | 1.5412 | 91% |
| 100 : 61 | 1 : 5.08 | 1.5289 | 1.5329 | Not possible |
| 100 : 80 | 1 : 6.75 | 1.5236 | 1.5272 | Not possible |

studied [50]. For this purpose, silanized precipitated silica nanoparticles with a spherical shape and an average diameter of 14 nm (Nanoresins AG, Geesthacht), which are generally supposed to have mostly a topological impact on the epoxy network but essentially no chemical influence on the polymerization, are added to the epoxy reactants [25, 51]. In figure 5, the $n(u)$ curves of the pure, almost stoichiometric epoxy (100/14) and a nanocomposite based on the same epoxy composition but containing 67 mass parts of silica nanoparticles are compared. Obviously, the presence of nanoparticles neither removes the flattening of the $n(u)$ curve caused by the density saturation in I3 nor changes the slope in I1. From these observations we conclude that the effects of mass density on the refractive index are essentially not modified by the nanoparticles. It is plausible that the linear increase in $n(u)$ in I1 is solely linked to an increase in mass density with chemical conversion. However, in interval I2 the positive excess refractive index, which adds to the purely linear $n(u)$-background observed in I1, vanishes in the presence of the nanoparticles, so that for the nanocomposite the linear $n(u)$-behavior of zone I1 extends until I3. Also in I2 the linear background of the electronic polarizability at optical frequencies is attributed to the dipole number density, being roughly proportional to the mass density. Other contributions of optical polarizability, which are responsible for the positive excess refractive index in I2, have to be added for the pure epoxy (100/14). At the moment, it seems that the origins of the latter contributions can be disturbed by the nanoparticles so that the positive excess polarizability in I2 vanishes for the nanocomposite.

It appears that the linear increase in $n(u)$, i.e. $\rho(u)$, in I1 is observed for epoxies still possessing low average molecular weights. At this early stage of polymerization, a heterogeneous formation of dimers, trimers and $m$-mers that in essence do not interact with each other takes place. For strongly understoichiometric and overstoichiometric pure epoxy compositions, this linear regime I1 extends to rather high degrees of polymerization as the

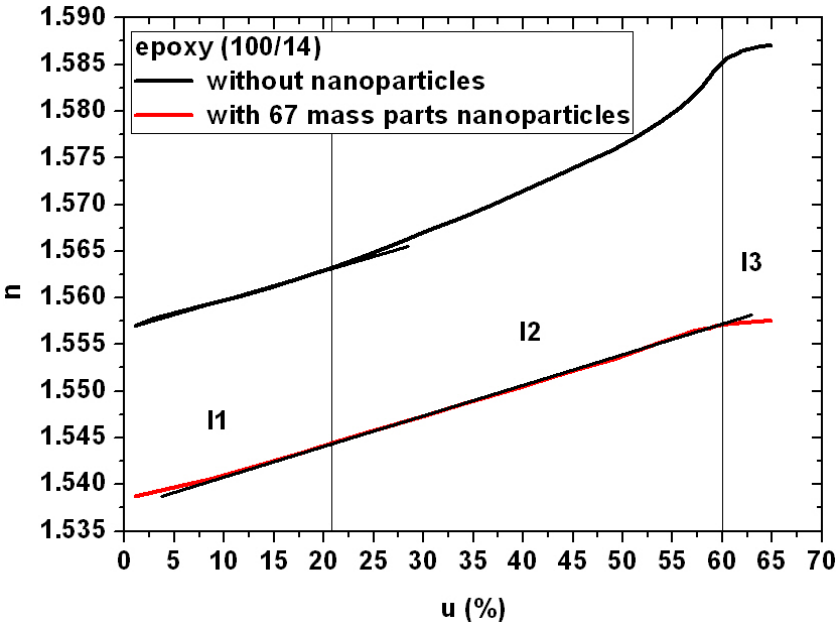


**Figure 5.** Refractive index versus chemical conversion $n(u)$ during the polymerization of an almost stoichiometric epoxy (100/14) and the same epoxy composition (100/14) loaded with 67 mass part silica nanoparticles. The preparation technique described in [50] explains the slight differences in $n(u)$ between the pure epoxy (100/14) indicated here and that shown in figure 4(a).

increase in the sample's average molecular weight as a function of chemical conversion is slowed down. As shown in table 1, for these highly unstoichiometric systems the percolation threshold of the epoxy network is either obtained for high chemical conversions or is even impossible. It seems that the linear regime can also spread to higher average molecular weights for almost stoichiometric samples when the macroscopically extended molecular network becomes strongly coarse grained due to the presence of 25 vol.% silica nanoparticles. Thus, the negligible electromagnetic interaction of molecules observed for small molecular groups in I1 can also be suppressed in a macroscopic network (i.e. in I2) in the presence of a sufficient amount of silica nanoparticles.

The linear increase in the refractive index as a function of mass density suggests the applicability of the Lorentz–Lorenz equation [33, 34, 41, 42] (see equation (2)) with a constant specific refraction $r$ for the given epoxy composition. Since for this epoxy $n$ is a weakly varying function of $u$ (total change smaller than 2%), it follows that $\mathrm{d}n/\mathrm{d}u$ is in good approximation proportional to $\mathrm{d}\rho/\mathrm{d}u$ by

$$\frac{\mathrm{d}\rho}{\mathrm{d}u} = \frac{1}{r}\frac{6n}{(n^2+2)^2}\frac{\mathrm{d}n}{\mathrm{d}u} \approx \mathrm{const}\frac{\mathrm{d}n}{\mathrm{d}u}. \tag{4}$$

The accuracy of this approximation scales with the total change in $n$, i.e. here roughly 2%. Obviously, the slope of $n(u)$ for the various systems depends on several effects, such as e.g. dilution effects for a high DGEBA or DETA concentration, compared to the stoichiometric

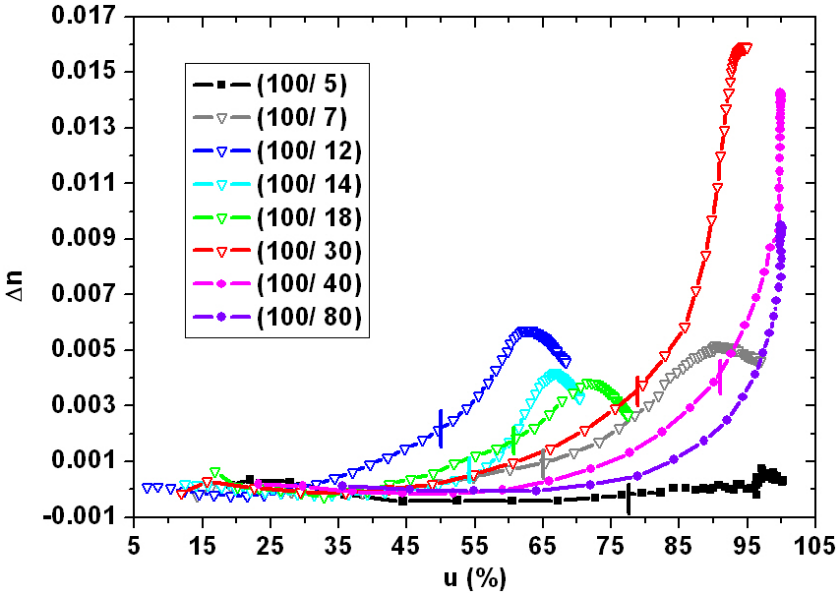


**Figure 6.** Excess refractive index $\Delta n(u) = n(u) - n|_x^{\mathrm{I1}}(u)$ for a representative selection of compositions versus the chemical conversion $u$. The vertical markers indicate the Flory–Stockmayer prediction of the sol–gel transition.

composition, and the respective molecular structural formation. Of course, the molecular structure depends also on the reactant's composition, but is also affected by the unequal reactivity of primary and secondary amines [16, 48, 52].

The remaining question concerns the interpretation of the nonlinear increase in $n(u)$ in the interval I2 (see figure 4). It should be stressed that this $n(u)$-anomaly is a specific property of certain DGEBA/DETA systems as it is not noticed in other gelating polymers, such as polyurethanes [53] and polydimethylsiloxanes (unpublished). As explained above, the cause of this increase in I2 most probably lies in a combination of an increasing average strength of the dipoles and an increasing dipole number density. From the above debate about the action of silica nanoparticles on the $n$-anomaly, we conclude that the linear background caused by the mass density augmentation is supposed to continue from I1 until the end of I2. Secondly, this linear contribution is superimposed by a nonlinearly increasing contribution to $n$ due to an increasing effective strength of the optical dipole system. In order to separate both these contributions in I2, the linear $n(u)$-relationship visible in I1 is extrapolated until the highest degree of polymerization and subtracted from the measured curves. A representative choice of the resulting excess refractive index curves $\Delta n(u) = n(u) - n|_{\mathrm{x}}^{\mathrm{I1}}(u) = n(u) - a_x - b_x \cdot u$ is displayed in figure 6. In interval I1, all $\Delta n$-curves are, of course, equal to zero within the margin of error. Except for the composition (100/5), the subsequent excess polarizability contribution leads to a strong, monotonous augmentation of $\Delta n$. Finally, for the vitrifying epoxies from (100/7) to (100/30), $\Delta n$ shows a maximum that reflects the leveling of $n(u)$ close to the glass transition. The subsequent apparent decrease in $\Delta n(u)$ in I3 is an artifact of the data treatment. In fact, it is due to the ignorance of the density-determined refractive index saturation in the chemically induced glassy state where indeed $\Delta n(u)$ becomes constant. According to figure 6, the most remarkable increases in $\Delta n$ occur for systems with no or little interference with the chemically induced glass transition. In those cases, an almost diverging increase in $\Delta n(u)$ is

experimentally evidenced. Since vitrification can be excluded as an inherent cause of $\Delta n(u)$, it is reasonable to discuss the question whether the sol–gel transition could be at the origin of the quasi-diverging $\Delta n$. Indeed, the significant growth in $\Delta n(u)$ seems to be inherently connected to network formation in the course of gelation. In order to get a rough overview of the location of the critical conversion $u_{sg}$, a suitable gelation theory like the one of Flory and Stockmayer [12, 16] will be applied. The critical conversion is calculated according to

$$u_{sg} = \sqrt{\frac{N_A f_A}{N_E f_E (f_A - 1)(f_E - 1)}}, \tag{5}$$

with $N_E$ and $N_A$ denoting the mole numbers of oxirane rings and amine hydrogens, and $f_A$ and $f_E$ being their respective functionalities. Using $f_A = 5$ and $f_E = 2$, the values of $u_{sg}$ were calculated for the studied epoxy compositions and listed in table 1.

Figure 6 shows for most systems a rough correlation between the onset of the steepest part of $\Delta n(u)$ and $u_{sg}$. On the other hand, it turns out that the strongly overstoichiometric systems (100/61) and (100/80) surely do not reach the gel state (see table 1). It is therefore likely that the actual appearance of the sol–gel transition is not a prerequisite for the existence and growth of $\Delta n(u)$. It remains unclear whether the sol–gel transition modifies the habit of the $\Delta n(u)$-curves. That the onset of $\Delta n(u)$ is observed for the smallest chemical conversion in the case of the stoichiometric composition gives a clear hint that the excess polarizability is linked to the formation of larger network aggregates.

For the vitrifying compositions from (100/7) to (100/30), the glass transition obviously truncates the $\Delta n(u)$ increase being characteristic for I2. As, for these systems, the sol–gel transition probably suffers a few per cent conversion prior to the glass transition, an interference of both transitions is likely. The chemically induced glass transition limits the further growth of $\Delta n$, but does not seem to reduce the currently existing excess polarizability. Interestingly, $\Delta n$ is maximal for the composition (100/30), which freezes only when an almost full degree of polymerization is reached. In other words, the gelation, i.e. the necessary condition for the excess polarizability contribution, could largely develop in this epoxy. In contrast with the influence of vitrification on $\Delta n(u)$, figure 5 shows that the addition of a sufficient amount of silica nanoparticles destroys the excess refractive index.

According to these statements, the origin of the optical excess polarization leading to $\Delta n(u)$ remains puzzling and the interpretation of this effect is necessarily speculative: it is argued that the optically excited molecular dipoles do cooperatively interact as long as they are arranged closely in an undisturbed molecular epoxy network. Apart from densification effects due to the structural formation accompanying the polymerization process, dipole–dipole interactions create the observed surplus of $n(u)$ in I2. In other words, the formation of large molecular network aggregates as well as structure-specific interactions between the molecular dipoles produce a dielectric situation in which positive feedback between these dipoles exists. However, these cooperative dipole interactions are weak since a sufficient amount of small topological and dielectric defects like silica nanoparticles are able to destroy them completely.

On the background of the 'feedback hypothesis', the interesting issue arises whether the onset of $\Delta n$ is gradual as a function of the chemical conversion or whether a critical size and/or density of the molecular network aggregates is needed in order to activate the excess polarization process. The data given in figure 6 seem to be in favor of a sudden onset of $\Delta n$. Although for

the highly understoichiometric epoxy (100/5) the sol–gel transition is predicted for $u = 77\%$ according to the Flory–Stockmayer theory, no excess refractive index $\Delta n$ is observed. Probably the necessary critical size and/or density of molecular aggregates cannot be reached for this composition.

The fact that strongly overstoichiometric compositions like the epoxy (100/80), which do not percolate, still develop a significant excess refractive index is related to the presence of a sufficient amount of adequate molecular network aggregates (microgels). As expected, figure 6 reveals that the amplitude of $\Delta n$ decreases significantly for an increasing overstoichiometry.

## 4. Conclusion

Different compositions of DGEBA/DETA-based epoxies were investigated by infrared spectroscopy and refractometry. The representations of the chemical conversion $u$ as well as of the refractive index $n$ versus time both give a rough view of the structural formation during the polymerization process. The reaction velocity $v_r(u)$ derived from the chemical conversion gives, in addition, a good overview of the composition-dependent chemically induced vitrification, but no indication of the gelation process.

On the other hand, the representation of the refractive index versus the chemical conversion turned out to be sensitive not only to the freezing but also to the gelation process. The evolution of $n(u)$ can be divided into three distinctive intervals reflecting different stages of structural formation. The first interval reflects the initial growth of the epoxy network molecules. The linear increase in the refractive index is related to the accompanying increase in mass density. The third interval, which is close to maximum conversion, is attributed to the chemically induced freezing process. In this interval, the refractive index evolution is predominantly coupled to that of the mass density that is triggered by the chemical freezing process.

Finally, in the intermediate interval, in which predominantly gelation takes place, two astonishing different processes contribute to the optical polarizability and consequently to the refractive index. As in the first interval, the increase in mass density accompanying the polymerization still yields a linear increase in the refractive index $n(u)$. In addition to this contribution, an unexpected nonlinear contribution to the refractive index is identified that is attributed to feedback between optically induced dipoles specific for molecular epoxy network aggregates, which are sufficiently large and/or dense. A unique relation between the evolution of the excess refractive index and the sol–gel transition was not found.

## Acknowledgments

We thank Professor Wilhelmi and Professor Klee for fruitful discussions. This work was financially supported by the University of Luxembourg, especially the project ‘Static and dynamic properties of nanocomposites’, and by the National Research Fund of Luxembourg.

## References

[1] Krüger J K 2007 About the nature of the structural glass transition: An experimental approach *Ageing and the Glass Transition* ed M Henkel *et al* (Berlin: Springer)

[2] Bat E, Grijpma D W and Feijen J 2008 Thermoreversible gelation behaviour of PTMC–PEG–PTMC triblock copolymers *J. Control. Release* **132** e37–9

[3] Eloundou J-P, Gerard J-F, Harran D and Pascault J P 1996 Temperature dependence of the behavior of a reactive epoxy-amine system by means of dynamic rheology. 2. High-Tg epoxy-amine system *Macromolecules* **29** 6917–27
[4] Firoozmand H, Murray B S and Dickinson E 2009 Microstructure and rheology of phase-separated gels of gelatin+oxidized starch *Food Hydrocolloids* **23** 1081–8
[5] Paquien J-N, Galy J, Gérard J-F and Pouchelon A 2005 Rheological studies of fumed silica-polydimethylsiloxane suspensions *Colloids Surfaces* A **260** 165–72
[6] Shenoy A V 1999 *Rheology of Filled Polymer Systems* (Dordrecht: Kluwer)
[7] Cadenato A, Salla J M, Ramis X, Morancho J M, Marroyo L M and Martin J L 1997 Determination of gel and vitrification times of thermoset curing process by means of TMA, DMTA and DSC techniques—TTT diagram *J. Therm. Anal.* **49** 269–79
[8] de Gennes P G 1979 *Scaling Concepts in Polymer Physics* (London: Cornell University Press)
[9] Krüger J K, Britz T, Le Coutre A, Baller J, Possart W, Alnot P and Sanctuary R 2003 Different glassy states, as indicated by a violation of the generalized Cauchy relation *New J. Phys.* **5** 80.1–80.11
[10] Donth E 2001 *The Glass Transition* (Berlin and Heidelberg: Springer)
[11] Zarzycki J 1982 *Les verres et l'état vitreux* (Paris: Masson)
[12] Adolf D, Martin J E and Wilcoxon J P 1990 Evolution of structure and viscoelasticity in an epoxy near the sol–gel transition *Macromolecules* **23** 527–31
[13] Martin J E and Adolf D 1991 The sol–gel transition in chemical gels *Annu. Rev. Phys. Chem.* **42** 311–39
[14] Volponi R, Corezzi S and Fioretto D 2007 Correlation between structural relaxation and distribution of particle clusters in glass-forming epoxy–amine mixtures undergoing step polymerization *Macromolecules* **40** 3450–60
[15] Mounif E, Bellenger V and Tcharkhtchi A 2008 Time–temperature–transformation (TTT) diagram of the isothermal crosslinking of an epoxy/amine system: curing kinetics and chemorheology *J. Appl. Polym. Sci.* **108** 2908–16
[16] Pascault J-P, Sautereau H, Verdu J and Williams R J J (ed) 2002 *Thermosetting Polymers* (New York: Marcel Dekker)
[17] Harsch M, Herzog F and Karger-Kocsis J 2008 Cure-induced normal force development in unfilled and filled epoxy resins *J. Compos. Mater.* **42** 2299–309
[18] Casalini R, Corezzi S, Livi A, Levita G and Rolla P A 1997 Dielectric parameters to monitor the crosslink of epoxy resins *J. Appl. Poly. Sci.* **65** 17–25
[19] Kroutilová I, Matejka L, Sikora A, Soucek K and Stas L 2006 Curing of epoxy systems at sub-glass transition temperature *J. Appl. Polym. Sci.* **99** 3669–76
[20] Núnez-Regueira L, Gracia-Fernández C A and Gómez-Barreiro S 2005 Use of rheology, dielectric analysis and differential scanning calorimetry for gel time determination of a thermoset *Polymer* **46** 5979–85
[21] Thomas R, Durix S, Sinturel C, Omonov T, Goossens S, Groeninckx G, Moldenaars P and Thomas S 2007 Cure kinetics, morphology and miscibility of modified DGEBA-based epoxy resin—effects of a liquid rubber inclusion *Polymer* **48** 1695–710
[22] Xie M, Zhang Z, Gu Y, Li M and Su Y 2009 A new method to characterize the cure state of epoxy prepreg by dynamic mechanical analysis *Thermochim. Acta* **487** 8–17
[23] Min B G, Stachurski Z H and Hodgkin J H 1993 Cure kinetics of elementary reactions of a DGEBA/DDS epoxy resin: 1. Glass transition temperature versus conversion *Polymer* **34** 4908–12
[24] Paz-Abuin S, Pellin M P, Paz-Pazos M and Lopez-Quintela A 1997 Influence of the reactivity of amine hydrogens and the evaporation of monomers on the cure kinetics of epoxy-amine: kinetic questions *Polymer* **38** 3795–804
[25] Baller J, Becker N, Ziehmer M, Thomassey M, Zielinski B, Müller U and Sanctuary R 2009 Interactions between silica nanoparticles and an epoxy resin before and during network formation *Polymer* **50** 3211–9

[26] Sanctuary R, Baller J, Zielinski B, Becker N, Krüger J K, Philipp M, Müller U and Ziehmer M 2009 Influence of $Al_2O_3$ nanoparticles on the isothermal cure of an epoxy resin *J. Phys.: Condens. Matter* **21** 035118
[27] Philipp M, Sanctuary R, Baller J, Zielinski B and Krüger J-K 2007 *Beiträge zur Experimentalphysik, Didaktik und computergestützten Physik* (Berlin: Logos Verlag) p 20
[28] Possart W, Krüger J K, Wehlack C, Müller U, Petersen C, Bactavatchalou R and Meiser A 2006 Formation and structure of epoxy network interphases at the contact to native metal surfaces *C. R. Chim.* **9** 60–79
[29] Wehlack C, Possart W, Krüger J K and Müller U 2007 Epoxy and polyurethane networks in thin films on metals—formation, structure, properties *Soft Mater.* **5** 87–134
[30] Mijovic J and Andjelic S 2002 A study of reaction kinetics by near-infrared spectroscopy. 1. Comprehensive analysis of a model epoxy/amine system *Macromolecules* **28** 2787–96
[31] Herraez J V and Belda R 2006 Refractive indices, densities and excess molar volumes of monoalcohols plus water *J. Solution Chem.* **35** 1315–28
[32] Iglesias-Otero M A, Troncoso J, Carballo E and Romani L 2008 Density and refractive index in mixtures of ionic liquids and organic solvents: correlations and predictions *J. Chem. Thermodyn.* **40** 949–56
[33] Lorentz H A 1880 *Wied. Ann. Phys.* **9** 641–65
[34] Lorenz L V 1880 *Wied. Ann. Phys.* **11** 70–103
[35] Francesconi R and Ottani S 2007 Correlation of density and refraction index for liquid binary mixtures containing polyglycols. Use of the group contributions in the Lorentz–Lorenz, Gladstone–Dale and Vogel equations to evaluate density of mixtures *J. Mol. Liquids* **133** 125–33
[36] Venermo J and Sihvola A 2005 Dielectric polarizability of circular cylinder *J. Electrost.* **63** 101–17
[37] Sihvola A, Venermo J and Yla-Oijala P 2004 Dielectric response of matter with cubic, circular-cylindrical, and spherical microstructure *Microw. Opt. Technol. Lett.* **41** 245–8
[38] Hoenders B J 2007 *The painful derivation of the refractive index from microscopical considerations 2nd Int. Engineer. Conf. on Light-Activated Tissue Regeneration and Therapy* ed R Waynant (Tomar, Portugal: Springer) pp 297–305
[39] Philipp M, Gervais P C, Sanctuary R, Müller U, Baller J, Wetzel B and Krüger J K 2008 Effect of mixing sequence on the curing of amine-hardened epoxy/alumina nanocomposites as assessed by optical refractometry *Express Polym. Lett.* **2** 546–52
[40] Krishnaswamy R K and Janzen J 2005 Exploiting refractometry to estimate the density of polyethylene: the Lorentz–Lorenz approach re-visited *Polym. Test.* **24** 762–5
[41] Liu Y G and Daum P H 2008 Relationship of refractive index to mass density and self-consistency of mixing rules for multicomponent mixtures like ambient aerosols *J. Aerosol Sci.* **39** 974–86
[42] Sharma S, Patel P B, Patel R S and Vora J J 2009 Density and viscosity study of binary mixtures of eucalyptol with methanol, ethanol, 1-propanol, 1-butanol and 2-methylpropan-1-ol at 303.15, 308.15 and 313.15 K *J. Indian Chem. Soc.* **86** 419–24
[43] Giner B, Villares A, Lopez M C, Royo F M and Lafuente C 2005 Refractive indices and molar refractions for isomeric chlorobutanes with isomeric butanols *Phys. Chem. Liq.* **43** 13–23
[44] Tekin N, Cebe M and Tarimci C 2004 Polarizabilities and dipole moments of benzaldehyde, benzoic acid and oxalic acid in polar and nonpolar solvents *Chem. Phys.* **300** 239–46
[45] Born M and Wolf E 1999 *Principles of Optics* (Cambridge: Cambridge University Press)
[46] Müller U, Bactavatchalou R, Bailer J, Philipp M, Sanctuary R, Zielinski B, Alnot P, Possart W and Krüger J K 2008 Acoustic profilometry of interphases in epoxy due to segregation and diffusion using Brillouin microscopy *New J. Phys.* **10** 023031
[47] Krevelen D W and Hoftyzer P J 1976 *Properties of Polymers: Their Estimation and Correlation with Chemical Structure* (Amsterdam: Elsevier)
[48] Lee H and Neville K 1967 *Handbook of Epoxy Resins* (New York: McGraw-Hill)
[49] Mijovic J and Wijaya J 1994 Reaction kinetics of epoxy/amine model systems: the effect of electrophilicity of amine molecule *Macromolecules* **27** 7589–600

[50] Philipp M, Sanctuary R, Gervais P-C, Wehlack C, Possart W, Müller U, Kieffer J and Krüger J K 2010 Influence of nanoparticles on the coupling strength between optical polarisability and structural formation during the chemically induced sol-gel and glass transitions of epoxy/silica nanocomposites *J. Phys. Chem. B* submitted

[51] Kinloch A J, Mohammed R D, Taylor A C, Eger C, Sprenger S and Egan D 2005 The effect of silica nano particles and rubber particles on the toughness of multiphase thermosetting epoxy polymers *J. Mater. Sci.* **40** 5083–6

[52] Paz-Abuin S, Lopez-Quintela A, Varela M, Pazos-Pellin M and Prendes P 1997 Method for determination of the ratio of rate constants, secondary to primary amine, in epoxy-amine systems *Polymer* **38** 3117–20

[53] Philipp M, Vergnat C, Müller U, Sanctuary R, Baller J, Possart W, Alnot P and Krüger J K 2009 Second order elasticity at hypersonic frequencies of reactive polyurethanes as seen by generalized Cauchy relations *J. Phys.: Condens. Matter* **21** 035106